IOP Publishing

Plasma Physics and Controlled Fusion

Plasma Phys. Control. Fusion **56** (2014) 015002 (9pp)

doi:10.1088/0741-3335/56/1/015002

Characterization of predator–prey dynamics, using the evolution of free energy in plasma turbulence

P Morel[1,2], **Ö D Gürcan**[1] **and V Berionni**[1]

[1] Laboratoire de Physique des Plasmas, Ecole Polytechnique, CNRS, UPMC, UPSud-XI, 91128 Palaiseau, France

[2] Laboratoire de Physique Statistique et des Plasmas, Université Libre de Bruxelles, CP 231, Bruxelles, Belgium

Received 9 January 2013, revised 9 October 2013
Accepted for publication 28 October 2013
Published 6 December 2013

Abstract

A simple dynamical cascade model for the evolution of free energy is considered in the context of gyrokinetic formalism. It is noted that the dynamics of free energy, that characterize plasma micro-turbulence in magnetic fusion devices, exhibit a predator–prey character. Various key features of predator–prey dynamics such as the time delay between turbulence and large-scale flow structures, or the intermittency of the dynamics are identified in the quasi-steady-state phase of the nonlinear gyrokinetic simulations. A novel prediction on the ratio of turbulence amplitudes in different parts of the wavenumber domain that follows from this simple predator–prey model is compared to a set of nonlinear simulation results and is observed to hold quite well in a large range of physical parameters. Detailed validation of the predator–prey hypothesis using nonlinear gyrokinetics provides a very important input for the effort to apprehend plasma micro-turbulence, since the predator–prey idea can be used as a very effective intuitive tool for understanding and designing efficient transport models.

Keywords: plasma turbulence, gyrokinetics, tokamaks, plasma simulation, predator–prey dynamics

(Some figures may appear in colour only in the online journal)

1. Introduction

Predator–prey dynamics constitute a common paradigm in natural sciences that provides a powerful perspective for the interpretation of various complex phenomena [1]. In the context of fusion plasmas, the paradigm offers an important alternative insight into the dynamical behavior of micro-turbulence, believed to be responsible for the anomalous transport, and the self-regulating sheared flows that are driven by this micro-turbulence, and which control the anomalous transport [2]. The evolution of turbulence and zonal flows (ZFs) that it drives may eventually explain the dynamical coupling leading to the low to high confinement (L–H) transition [2, 3] in magnetic fusion devices. Interesting quasi-periodic activity, which may be linked to the predator–prey oscillations between turbulence and large-scale flows in the form of mean or ZFs or geodesic acoustic modes, (GAMs) has been observed recently in a number of machines prior to and during the L–H transition [4–6].

The predator–prey dynamics also play an important role in the nonlinear cascade process via the refraction of the turbulence in the low-k (k being the wavenumber) energy containing scales to high-k dissipation scales by the self-generated ZFs [7–9]. Interplay between ZFs and plasma micro-turbulence is well known and has been widely observed in various gyrokinetic simulations [10–13]. This mediating role of ZFs for the cascade of free energy has also recently been observed in gyrokinetic simulations [14].

The predator–prey dynamics in gyrokinetic turbulence is characterized by analyzing gyrokinetic nonlinear simulations performed with the GENE code. Time traces of zonal and nonzonal free energies are analyzed in terms of their cross-correlation, showing a clear time delay between the zonal free energy and the rest of the turbulence. This first clue of a predator–prey dynamic is complemented by the kurtosis of the free energy spectrum along binormal wavevector. The latter clearly suggests a two domain scale separation along the binormal wavevector, with an important intermittency at intermediate, energy containing scales, while the smallest dissipation scales are found very close to Gaussian distribution in time. The results allow to design a three domain predator–prey model that is tested successfully with respect to theoretical predictions.

The gyrokinetic description is presented in section 2, where the free energy, which is a quadratically conserved quantity in gyrokinetic framework, is introduced. Predator–prey oscillations are evidenced during gyrokinetic simulations of ion temperature gradient (ITG) driven turbulence in section 3, and the statistics of each Fourier mode along binormal direction are analysed. A comparison between a simple three population dynamical model [9] and various gyrokinetic simulations is given in section 4.

2. Gyrokinetic description

Plasma turbulence in a strong magnetic field can be described by the gyrokinetic equation [19–30], which by filtering the rapid gyromotion, reduces the Vlasov equation to an equation governing the evolution of the five-dimensional guiding-center distribution function $f = f(\boldsymbol{R}, v_\parallel, \mu, t)$, where $\boldsymbol{R}$ is the guiding-center coordinate, $v_\parallel$ is the velocity coordinate along the magnetic field B_0 and $\mu = m_i v_\perp^2/(2B_0)$ is the magnetic moment, which is an adiabatic invariant. As will be presented in the following section, this invariance allows the reduction of the gyrokinetic Vlasov equation to a four-dimensional advection in phase space, while the magnetic moment μ can be simply considered as a label. This consideration holds for the *collisionless* gyrokinetic system of equations, while adding the effect of collisions can complicate the problem. Since the pioneering works on the gyrokinetic formulation [19–27] and the first attempts of numerical resolution of the gyrokinetic equations [10, 23, 31], gyrokinetics solvers have become important tools for a fundamental understanding of turbulence in magnetized plasmas [33]. Exhaustive modern reviews on the gyrokinetic equation and the associated plasma micro-turbulence are available for the reader interested in delving further into this subject [32–34].

2.1. Gyrokinetic equations

The total ion guiding-center distribution function $f(\boldsymbol{R}, v_\parallel, \mu, t)$ is split between fluctuations and a Maxwellian equilibrium $f = F_0 + \delta f$ with ($F_0 = \mathrm{e}^{-v_\parallel^2 - \mu B_0}$). In the local version of the GENE code employed for this study [35], a field aligned coordinate system is used ($\boldsymbol{R} \to x, y, z$ with z the field aligned, x the radial and y the binormal coordinates), and the fields are Fourier transformed in the plane perpendicular to the background magnetic field ($x,\ y \to k_x,\ k_y$). The gyrokinetic system of equations governing the dynamics of ion guiding-center distribution function f_k reads

$$\partial_t \delta f_k + \left(v_\parallel \partial_z + \mathrm{i}\omega_{B_0}\right) \delta h_k + a_\parallel \partial_{v_\parallel} \delta h_k = \mathrm{i}\omega_{*T_i} F_{0i}\, (J_0 \Phi)_k$$
$$+ \sum_{p+q=-k} \left(\hat{\boldsymbol{b}} \times \boldsymbol{p}.\boldsymbol{q}\right) (J_0\Phi)_q^\star\, \delta h_p^\star - D[\delta f_k], \qquad (1)$$

where the notation $\delta h_k = \delta f_k + q_i F_0 (J_0\Phi)_k / T_{0i}$ has been used for brevity. Ions are characterized by an equilibrium density n_{i0} and a temperature T_{i0}. $v_{T_i} = \sqrt{2T_{i0}/m_i}$, $\Omega_{ci} = q_i B_0/m_i$ and $\rho_i = v_{T_i}/\Omega_{ci}$ are ion thermal velocity, cyclotron frequency and Larmor radius respectively. Ion temperature and density equilibrium profiles are contained in the density and temperature gradient lengths $L_n^{-1} = -n_{i0}^{-1}\mathrm{d}n_{i0}/\mathrm{d}r$ and $L_{T_i}^{-1} = -T_{i0}^{-1}\mathrm{d}T_{i0}/\mathrm{d}r$, that appear in the diamagnetic frequency $\omega_{*Ti} = \omega_{*i}(1 + \eta_i[v_\parallel^2 + \mu B_0 - 3/2]/v_{T_i}^2)$, via $\eta_i = L_n/L_{T_i}$ and $\omega_{*i} = -\rho_i k_y/L_n$. The magnetic curvature and gradient are taken into account in the associated frequency: $\omega_{B_0} = \rho_i v_{T_i}(v_\parallel^2 + \mu B_0/2)(K_x k_x + K_y k_y)$ that contains the geometric prefactors K_x and K_y related to magnetic inhomogeneity. Details about the magnetic geometry can be found in [36]. Concentric circular flux surfaces are used in the present study. The dynamics parallel to the background magnetic field B_0 appear in the parallel acceleration: $a_\parallel = -v_{T_i}\mu\partial_z B_0/2$. As usual in gyrokinetics, the link between particles and guiding-center coordinates is provided by the gyroaverage operator, noted J_0 since it simplifies to the Bessel function in k space: $J_0 = J_0(k_\perp v_\perp/\Omega_{ci})$, where $k_\perp(z)$ is the perpendicular wavenumber, and $v_\perp^2(z, \mu) = \mu B_0(z)/(2T_{i0})$. The nonlinear term associated to advection due to the $\boldsymbol{E} \times \boldsymbol{B}$ velocity read

$$N[\delta f_k,\ (J_0\phi)_k] = \sum_{p+q=-k} \left(\hat{\boldsymbol{b}} \times \boldsymbol{p}.\boldsymbol{q}\right) (J_0\phi)_q^\star\, \delta h_p^\star.$$

Dissipative processes are modeled in this work by hyperdiffusion operators, and the dissipation term takes the general form:

$$D[\delta f_k] = c_\perp k_\perp^{2n} \delta h_k + c_z \partial_z^4 \delta h_k + c_{v_\parallel} \partial_{v_\parallel}^4 \delta h_k,$$

dependence of the micro-turbulence characteristics when varying c_z and $c_{v_\parallel}$ has been intensively studied in [37], and the standard values of the amplitudes for studying ion micro-turbulence with adiabatic electrons are $c_z = 1.0$, $c_{v_\parallel} = 1.0$ and $c_\perp = 0.0$. The $c_\perp$ value can be adjusted in order to minimize the perpendicular grid (k_x, k_y), corresponding to gyrokinetic large eddy simulation (GyroLES) methods [18]. Two values of n are considered in the following, $n = 1$ leading to a diffusion operator, while $n = 2$ corresponds to a hyperdiffusion one.

The coupling between the ion guiding-center distribution function δf_k and the electrostatic potential Φ_k is ensured by the quasi-neutrality equation:

$$\pi B_0 \int \mathrm{d}\mu \mathrm{d}v_\parallel\, (J_0 \delta f)_k$$
$$= \widetilde{\Phi}_k + Z_i \frac{T_{e0}}{T_{i0}} \left[1 - \Gamma_0\left(\frac{v_{T_i}^2 k_\perp^2}{\Omega_{ci}^2}\right)\right] \Phi_k, \qquad (2)$$

where electrons have been assumed adiabatic with temperature T_{e0} (with $T_{i0} = T_{e0}$ in the following). Here, $\widetilde{\Phi}_k = \Phi_k - \langle\Phi_k\rangle$, where $\langle\Phi_k\rangle$ is the flux surface averaged electrostatic potential. $\Gamma_0(v_{T_i}^2 k_\perp^2/\Omega_{ci}^2)$ is the modified Bessel function.

Simulations that we present in the following are performed using the GENE code [35, 38]. Despite the fact that GENE is also adapted for electromagnetic and global problems [39], the direct numerical simulations (DNSs) presented here are restricted to local electrostatic ITG driven turbulence with adiabatic electrons.

2.2. Free energy: a gyrokinetic conserved quantity

The gyrokinetic equation, as written in (1), has a number of nonlinearly conserved quantities, one of which is the so-called free energy, whose budget can be written as:

$$\partial_t \mathcal{E} = \mathcal{G} - \mathcal{D}, \tag{3}$$

where:

$$\begin{aligned}
\mathcal{E} &= n_{i0} \int \mathrm{d}\Lambda_k \frac{\delta h_k^\star}{2F_0} \delta f_k, \\
\mathcal{G} &= n_{i0} \int \mathrm{d}\Lambda_k \frac{\delta h_k^\star}{F_0} i\omega_{*Ti} F_{0i} \left(J_0 \Phi\right)_k, \\
\mathcal{D} &= n_{i0} \int \mathrm{d}\Lambda_k \frac{\delta h_k^\star}{F_0} D[\delta h_k],
\end{aligned}$$

define the free energy, its injection and dissipation respectively (using the phase space integration $\int \mathrm{d}\Lambda_k = \sum_{k_x,k_y} \int \frac{\pi}{V} \mathrm{d}z\, \mathrm{d}v_\parallel\, \mathrm{d}\mu$ with the volume $V = \sum_{k_x,k_y} \int \mathrm{d}z/B_0$). An important feature of the free energy balance equation is that only the background density and temperature gradients contained in ω_{*T_i} act as sources of free energy [40–42]. In contrast, parallel dynamics as well as magnetic field curvature and gradients only distribute the free energy between electrostatic and entropy terms [43]. The nonlinear term $N[\delta f_k, (J_0\Phi)_k]$ plays the role of transferring the free energy across the perpendicular scales [14, 44]. A local free energy balance in perpendicular Fourier space can be expressed as:

$$\partial_t \mathcal{E}_{\ell_\perp} = \mathcal{G}_{\ell_\perp} + \mathcal{N}_{\ell_\perp} - \mathcal{D}_{\ell_\perp}, \tag{4}$$

where $\ell_\perp$ may be taken to correspond to any partition of the perpendicular Fourier space (for example $k_{\perp\ell} < \ell_\perp < k_{\perp\ell+1}$), and the contribution of the nonlinear term satisfies $\sum_{\ell_\perp} \mathcal{N}_{\ell_\perp} = 0$.

2.3. The gyrokinetic large eddy simulation (GyroLES) technique

The large eddy simulation (LES) technique was primarily developed in the context of fluid (Navier–Stokes) turbulence. It consists in resolving only the largest scales of turbulence, while modeling the small scales by dissipative terms, which allows an important gain in numerical requirement. This technique has recently been extended to gyrokinetic turbulence [15, 18]. From a mathematical point of view, small scales can be filtered out by the action of a Fourier low-pass filter in the perpendicular Fourier space (k_x, k_y), and the filtered gyrokinetic equation can be expressed in terms of the filtered distribution function $\overline{\delta f_k}$:

$$\begin{aligned}
\partial_t \overline{\delta f_k} + \left(v_\parallel \partial_z + \mathrm{i}\omega_{B_0}\right) \overline{\delta h_k} + a_\parallel \partial_{v_\parallel} \overline{\delta h_k} &= \mathrm{i}\omega_{*T_i} F_{0i} \overline{(J_0\Phi)_k} \\
+ N[\overline{\delta f_k}, \overline{(J_0\Phi)_k}] - D[\overline{\delta f_k}] - T[\overline{\delta f_k}, \delta f_k], &
\end{aligned} \tag{5}$$

with the definition $\overline{\delta h_k} = \overline{\delta f_k} + q_i F_0 \overline{(J_0\Phi)_k}/T_{0i}$, and where a new term appears from the filtering of the nonlinear term:

$$T[\overline{\delta f_k}, \delta f_k] = N[\overline{\delta f_k}, \overline{(J_0\Phi)_k}] - \overline{N\left[\delta f_k, (J_0\Phi)_k\right]},$$

which is usually referred to as the sub-grid term, since it still involves δf_k and also requires the knowledge of the filtered smallest scales.

It has been shown that the role of the smallest scales is to dissipate free energy, and the sub-grid term can be modeled by a dissipation term that can be added to the usual dissipations: $D_{\mathrm{LES}}[\overline{\delta f_k}] = c_\perp k_\perp^{2n} \overline{\delta h_k}$, with $n = 1$ and $n = 2$, corresponding to a diffusion or respectively to a hyperdiffusion LES model.

In the following section 3, DNSs will first be considered, in order to describe numerically all the turbulent scales and observe in three cases the main features and insights of predator–prey dynamics. For more extended parametric studies that will be presented in section 4, GyroLES technique will be used.

3. Predator–prey oscillations in gyrokinetic turbulence

In this section, fundamentals of plasma micro-turbulence are analyzed in free energy terms. Importance of the ZFs, small and large scales perpendicular to the background magnetic field will be discussed and compared, in order to design a minimal predator–prey model for gyrokinetic turbulence.

3.1. Free energy interplay between ZFs and turbulence

In plasma turbulence, ZFs [45] are of special importance, since these structures, extended over a given flux surface, play a regulating role on the turbulence that generates them. By defining two domains in perpendicular Fourier space: $\overline{\ell_\perp}$ associated to ZFs ($k_y = 0$, $k_\parallel = 0$), and $\widetilde{\ell_\perp}$ associated to the rest of the turbulent scales, the ZF free energy $\overline{\mathcal{E}}$ can be separated from the rest of the drift wave turbulence $\tilde{\mathcal{E}}$, where the energy budget takes the form

$$\partial_t \overline{\mathcal{E}} = \overline{\mathcal{N}} - \overline{\mathcal{D}}, \tag{6}$$

$$\partial_t \widetilde{\mathcal{E}} = \widetilde{\mathcal{G}} + \widetilde{\mathcal{N}} - \widetilde{\mathcal{D}}. \tag{7}$$

It is important to note here that it is the free energy (which corresponds to potential enstrophy in the fluid limit) that is exchanged between the ZFs and the drift waves and not just the kinetic energy. The mechanism invoked here is not that of a classical inverse cascade but of a potential vorticity homogenization [46, 47], which manifests itself as disparate scale interactions in k-space [48]. Since there is no linear driving mechanism for the ZFs (i.e. $\overline{\mathcal{G}} = 0$), these structures feed on the free energy of the fluctuations and hence play the same regulating role on the underlying turbulence that a predator species plays on the population of a prey species.

DNSs have been performed for three values of $R_0/L_{T_i} = 6.0, 6.92, 8.0$, with other parameters being those of the ITG Cyclone Base Case [49] ($R_0/L_n = 2.22$, the safety factor: $q = 1.4$, the magnetic shear: $\hat{s} = 0.796$, the minor radius:

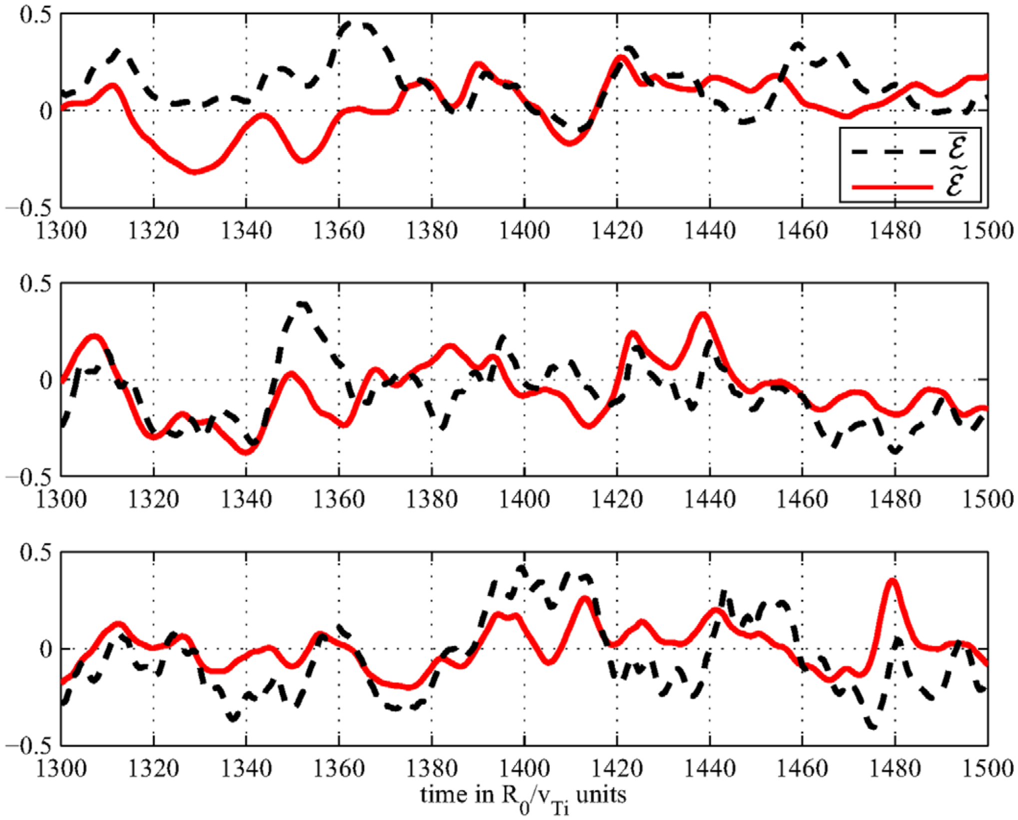

Figure 1. Time evolution of the normalized free energy $\overline{\mathcal{E}}$ associated with ZFs and $\widetilde{\mathcal{E}}$ associated with the rest of the turbulence, for three different values of $R_0/L_{T_i} = 6.0, 6.92, 8.0$ from top to bottom.

$r_0 = 0.18R_0$, and $T_{e0} = T_{i0}$). The associated grid sizes: $L_x \times L_y = 128 \times 128\rho_i^2$ in the plane perpendicular to the magnetic field, with a number of points $N_x \times N_y = 128^2$, the parallel and velocity domains are respectively: $L_z = 2\pi$, $L_{v_\parallel} = 6v_{T_i}$, $\mu = 9q_i\rho_i v_{T_i}$, corresponding to $N_z \times N_{v_\parallel} \times N_\mu = 16 \times 32 \times 8$ points.

Figure 1 represents the time evolution during turbulent phase of free energy components $\overline{\mathcal{E}}$ and $\widetilde{\mathcal{E}}$, that have been normalized to their mean, and where only a small fraction of the total time trace is represented in order to see the details of dynamics. As expected from a predator–prey interpretation [2], it can be observed that the free energy dynamics of the ZF and the turbulence are largely correlated. In order to check if this dynamic exhibits predator–prey features, one can look at the phase relation between these two quantities to see if there exists a time shift between the turbulence and the ZF free energy fluctuations.

The cross correlation in time between the ZF free energy and the rest of the turbulence can be defined as follows:

$$C(\Delta t) = \frac{\int \mathrm{d}t \left(\widetilde{\mathcal{E}}(t+\Delta t) - \langle\widetilde{\mathcal{E}}\rangle\right)\left(\overline{\mathcal{E}}(t) - \langle\overline{\mathcal{E}}\rangle\right)}{\sqrt{\int \mathrm{d}t \left(\widetilde{\mathcal{E}}(t) - \langle\widetilde{\mathcal{E}}\rangle\right)^2 \int \mathrm{d}t' \left(\overline{\mathcal{E}}(t') - \langle\overline{\mathcal{E}}\rangle\right)^2}},$$

where $\langle\overline{\mathcal{E}}\rangle$ and $\langle\widetilde{\mathcal{E}}\rangle$ represent the time averages of the free energy of the ZF and of the rest of the turbulence respectively.

The maximal value of the cross-correlation $C(\Delta t)$ corresponds to the mean time delay between the free energy of the ZFs $\overline{\mathcal{E}}$ and the free energy of the rest of the turbulence $\widetilde{\mathcal{E}}$.

In figure 2(a), cross-correlation between $\overline{\mathcal{E}}$ and $\widetilde{\mathcal{E}}$ is given as a function of the time lag. The average time delay Δt between $\overline{\mathcal{E}}$ and $\widetilde{\mathcal{E}}$ is given by the location of the maximal correlation in figure 2. The time delay is found not to depend on the logarithmic temperature gradient length, with an approximate value: $\Delta t \approx 2R_0/v_{T_i}$ in normalized units, or expressed in physical units: $\Delta t \approx 8\,\mu$s. The time delay is found negative, indicating that $\widetilde{\mathcal{E}}(t)$ precedes in time the ZF free energy $\overline{\mathcal{E}}(t)$: this gives the first clue for a predator–prey dynamic between the ZFs considered as a predator and the rest of the turbulence as the prey. As expected, the maximum levels of correlation, measured with this method, are in good agreement when varying the temperature gradient length.

ITG turbulence is mainly regulated by the value of the ITG length R_0/L_{T_i}, and linear stability analysis gives a critical value $(R_0/L_{T_i})_\mathrm{c} \approx 4$, which is observed to be upshifted due to nonlinear interactions $(R_0/L_{T_i})_\mathrm{c,exp} \approx 5.5$ [49]. Close to marginality, the ITG turbulence is dominated by the ZFs dynamics, displaying an intermittent behavior. The difference in the values of maximal correlation observed in figure 2 between high values of temperature gradient lengths $R_0/L_{T_i} = 6.9,\ 8.0$, and the value closer to marginality $R_0/L_{T_i} = 6.0$, can be explained by important slow time dynamics when close to marginality, that disappear when increasing the temperature gradient.

In figure 2(b), this effect is eliminated by subtracting from each turbulent signal its smooth filtered component: the

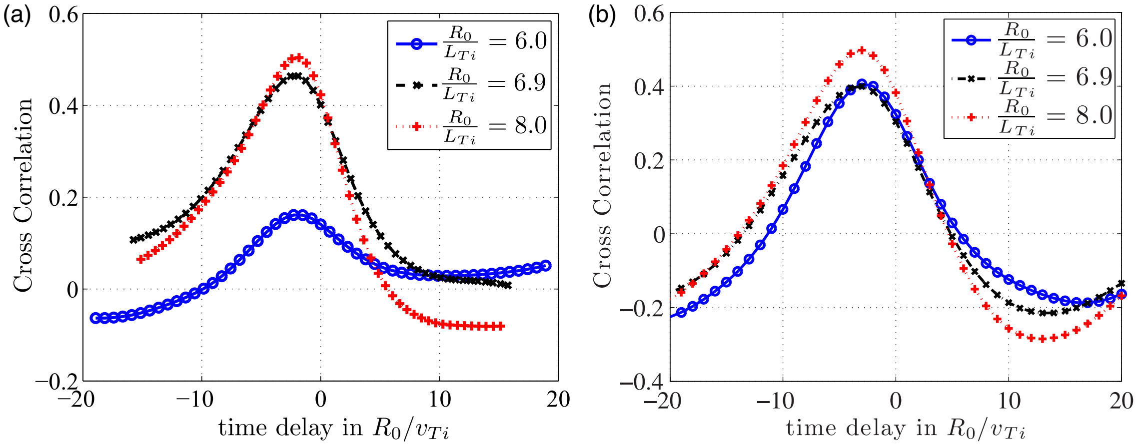

Figure 2. Cross-correlation between ZF and drift wave turbulent signals, for different values of the logarithmic temperature gradient R_0/L_{T_i} (*a*), and cross-correlation between ZFs and drift wave signals smoothed with a Gaussian filter of extent 50 time points (*b*).

resulting signal $\mathcal{X}_{\text{fast}}(t)$ can be expressed as follows:

$$\mathcal{X}_{\text{fast}}(t) = \mathcal{X}(t) - \int \mathrm{d}t'\kappa(t')\mathcal{X}(t - t'),$$

where $\mathcal{X}$ stands for ZFs ($\overline{\mathcal{E}}$) or drift waves ($\widetilde{\mathcal{E}}$) free energy, and the smooth filter $\kappa(t')$ is a Gaussian defined over 50 neighboring points. This procedure allows to remove the slow time dynamics from the signals, and the resulting cross-correlations between ZFs and drift wave fast signals are in good agreement, as illustrated in figure 2(*b*).

3.2. Statistics of binormal Fourier modes

The predator–prey type dynamics are also expected to have an intermittent nature. Therefore a look at the kurtosis κ is instructive:

$$\kappa = \frac{\frac{1}{n}\sum_i (x_i - \overline{x})^4}{\left(\frac{1}{n}\sum_{i=1}^{n} (x_i - \overline{x})^2\right)^2} - 3.$$

Indeed this latter quantity gives a measure of the deviation from Gaussian distribution for the discrete time signal x_i, where $\overline{x} = \frac{1}{n}\sum_{i=1}^{n} x_i$ is the mean and n the number of points. The Gaussian distribution is given by a kurtosis equal to zero, a positive value indicates a departure from Gaussian with heavier tails and a more acute peak around the mean (leptokurtic distributions), while a negative value indicates a distribution with tails thinner than Gaussian and a lower and broader peak around the mean (platykurtic). In particular, a positive kurtosis is a signature of a signal with intermittent behavior, which is very close to its mean most of the time, but presents also a relatively high probability for rare and high-amplitude events [50].

In figure 3, the kurtosis associated with the free energy spectrum $\mathcal{E}^{k_y}$ is plotted as a function of the binormal wavevector k_y for the same runs as in figure 1. This has been done during three nonlinear simulations (R_0/L_{T_i} = 6.0, 6.92, 8.0), by saving the time traces of each free energy Fourier mode $\mathcal{E}^{k_y}(t)$, and computing the kurtosis associated to each time signal. For all values of the temperature gradient, a clear separation is observed between the large and small

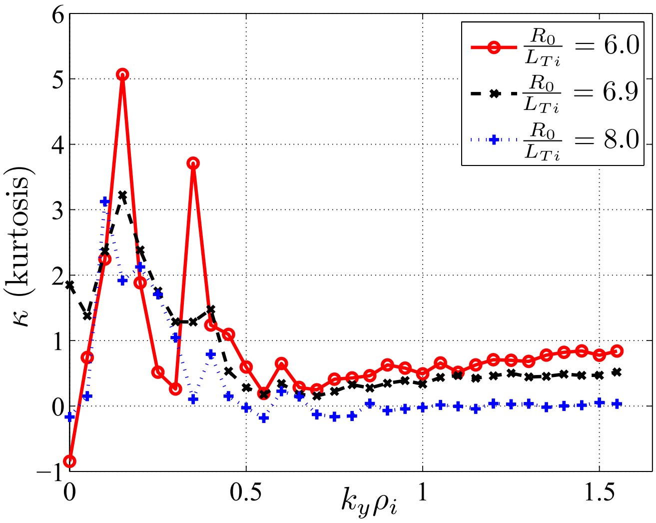

Figure 3. Free energy kurtosis κ as a function of the binormal wavevector $k_y\rho_i$, for different values of the logarithmic ITG R_0/L_{T_i}.

scales, where the statistics of the small scales are very close to Gaussian (corresponding to a kurtosis of 0), while the largest simulated scales associated with wavevectors $k_y\rho_i < 0.5$ show a clear departure from the Gaussian distribution, suggesting the presence of rare events with significant deviation from the mean. Moreover, decreasing the temperature gradient length R_0/L_{T_i}, the kurtosis of smallest scales also exhibits a mild departure from the Gaussian distribution, suggesting that the small scales of turbulence display weakly intermittent dynamics while approaching marginality.

The coupling between free energy producing scales and ZFs is a possible candidate to explain the higher intermittence of the large scales: the shearing by ZF strongly reduce turbulence at large scales by eddy breaking mechanism while the reduction of large-scale turbulence diminishes the preys available for the ZF to survive, leading to predator–prey dynamics. On the contrary, due to their size, the small scales are much less affected by this shearing effect. Finally, due to their intermittent nature, the statistics of the large scales appear to be very hard to capture, even with the very long time traces

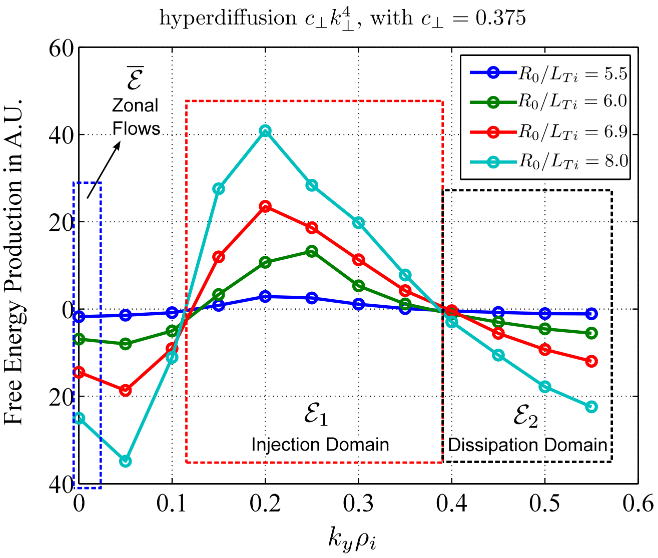

Figure 4. Free energy spectrum $\mathcal{E}^{k_y}$ for different values of the ITG R_0/L_{T_i}.

considered, and the behavior of largest scales only holds as a quantitative trend.

4. Gyrokinetic turbulence as a predator–prey system

While the usual predator–prey model already gives an interesting perspective on the dynamics (section 3.1), the fact that the predator–prey oscillations present the character of pulses in k-space is also important (section 3.2). Indeed, the free energy can be decomposed into the energy containing component (corresponding to the energy injection scales, associated to kurtosis far from Gaussian in figure 3), the dissipative component (corresponding to the dissipative scales, associated to kurtosis close to the Gaussian distribution in figure 3) and a ZF component, whose special role has been illustrated in figures 1 and 2. These three domains are illustrated in figure 4, where the time-averaged right-hand side of the free energy equation (4), i.e. $\mathcal{G}^{k_y} - \mathcal{D}^{k_y}$, is given for various values of the logarithmic temperature gradient R_0/L_{T_i}. Simulations have been performed on reduced grids $(N_x \times N_y = 48 \times 24)$ by means of the GyroLES technique [15] with a perpendicular hyperdiffusion model with $c_\perp = 0.375$. All others parameters are those of the DNSs presented in the previous section.

4.1. Gyrokinetic predator–prey model

The spectral transfer character of the predator–prey dynamics (6), (7) can be studied by using a model of the form

$$\partial_t \overline{\mathcal{E}} = \overline{\mathcal{N}} - \nu_F \overline{\mathcal{E}}, \tag{8}$$

$$\partial_t \mathcal{E}_1 = \mathcal{N}_1 + \gamma \mathcal{E}_1, \tag{9}$$

$$\partial_t \mathcal{E}_2 = \mathcal{N}_2 - \nu \mathcal{E}_2, \tag{10}$$

where, $\mathcal{E}_1$ is the free energy at the injection scale, $\mathcal{E}_2$ is the free energy at the dissipation scale and $\overline{\mathcal{E}}$ is the zonal free energy, and we have used the definitions: $\nu_F = \langle \overline{\mathcal{D}}/\overline{\mathcal{E}} \rangle$, $\gamma = \langle (\mathcal{G}_1 - \mathcal{D}_1)/\mathcal{E}_1 \rangle$ and $\nu = \langle (\mathcal{D}_2 - \mathcal{G}_2)/\mathcal{E}_2 \rangle$, where the brackets represent time averaging.

At this point, it is important to notice that the damping and growing k_y *scales* have not to be confused with linearly growing and damped *modes*, that are argued to be of special importance in self-regulation of plasma turbulence [16], and, are of interest here, in gyrokinetics [17]. Due to the high dimensionality of gyrokinetics, these modes are shown to coexist for a given k_y with linearly growing ones. Consistently, our definition of the parameters ν_F, γ and ν with respect to the free energy spectra $\mathcal{E}^{k_y}$ is summing in a same domain damped and linearly growing modes, resulting in a *net* turbulent damping or growth.

This three domain model is very similar to the model studied in [9], except that we use free energy here, in line with the gyrokinetic framework that we consider. As recently shown by [14] the free energy contribution of the nonlinear term can be expressed as a symmetrized triad transfer function: $\mathcal{N}_k = \sum_p \sum_q C_k^{p,q} \delta h_k \delta h_p \delta h_q$, where $C_k^{p,q}$ is an operator converting the modified distribution function δh_k into the electrostatic potential Φ_k. This allows us to write

$$\overline{\mathcal{N}} = \overline{\lambda}\, \overline{h} h_1 h_2, \tag{11}$$

$$\mathcal{N}_1 = \lambda_1 \overline{h} h_1 h_2, \tag{12}$$

$$\mathcal{N}_2 = \lambda_2 \overline{h} h_1 h_2. \tag{13}$$

where h_1, h_2 and $\overline{h}$ can be defined for instance using the partition $h_S = \sqrt{\int_S \mathcal{E}(k_\perp) d^2 k_\perp}$ where the domain S of integration in k-space is chosen to correspond to the injection, dissipation and zonal regions respectively. Although the model itself holds for any partition of the plane (k_x, k_y), the domain partition chosen for the numerical results presented in this work is defined along the k_y coordinate, while summing along k_x: the corresponding shell domains S correspond to slices along the k_y direction. It must be noted here, that the spectral density of free energy is defined as a velocity and parallel coordinate integral: $\mathcal{E}_{k_\perp} = n_{i0}\pi \int \mathrm{d}z\, \mathrm{d}\mu \mathrm{d}v_\parallel \delta h_k^\star \delta f_k / (2 V F_0)$.

Following [9], equations (8)–(10) can be averaged over the turbulent phase, so that time derivatives can be canceled since the gyrokinetic simulation reaches a quasi-stationary state as shown in figure 1. Coefficients λ_1, λ_2, $\overline{\lambda}$, γ, ν and ν_F are constants in time, and by eliminating the product $\langle \overline{h} h_1 h_2 \rangle$ in the averaged equations, the two following relations can be obtained:

$$\frac{\langle \mathcal{E}_1 \rangle}{\langle \overline{\mathcal{E}} \rangle} = -\frac{\lambda_1 \nu_F}{\overline{\lambda} \gamma}, \tag{14}$$

$$\frac{\langle \mathcal{E}_2 \rangle}{\langle \overline{\mathcal{E}} \rangle} = \frac{\lambda_2 \nu_F}{\overline{\lambda} \nu}. \tag{15}$$

It becomes evident from equation (14) that the geometrical prefactor λ_1 is negative, as could have been expected from figure 4. The two other coefficients $\overline{\lambda}$, and λ_2 are positive, recovering that the nonlinearity transfers free energy from injection scales to dissipative scales as well as to ZFs. Finally we have from equations (11)–(13) the different signs of the contributions of the nonlinear term in the free energy balance: $\overline{\mathcal{N}} > 0, \overline{\mathcal{N}}_1 < 0, \overline{\mathcal{N}}_2 > 0$.

4.2. Numerical tests of gyrokinetic predator–prey model

The parameters λ_1, λ_2 and $\bar{\lambda}$ correspond to geometrical prefactors depending on the choice of the k-space partition and the $C_{\boldsymbol{k}}^{p,q}$ that link Φ and h, and not on the physical parameters. In contrast, the linear growth rate corresponding to γ, the small-scale dissipation term ν, and the ZF drag ν_F are defined through $\mathcal{G}_{1,2}$, $\overline{\mathcal{G}}$, $\mathcal{D}_{1,2}$ and $\overline{\mathcal{D}}$, and thus are dependent on the free energy spectrum itself. Therefore, in principle, the net dependence of these coefficients on physical parameters such as the temperature gradient can be quite nontrivial. This point is investigated in figure 5, where the three parameters γ, ν_F and ν obtained from gyrokinetic numerical simulations, are represented as functions of the imposed R_0/L_{T_i}.

In figure 5, GyroLESs with various R_0/L_{T_i} are considered, with perpendicular hyperdiffusion amplitude $c_\perp = 0.5$, $n =$

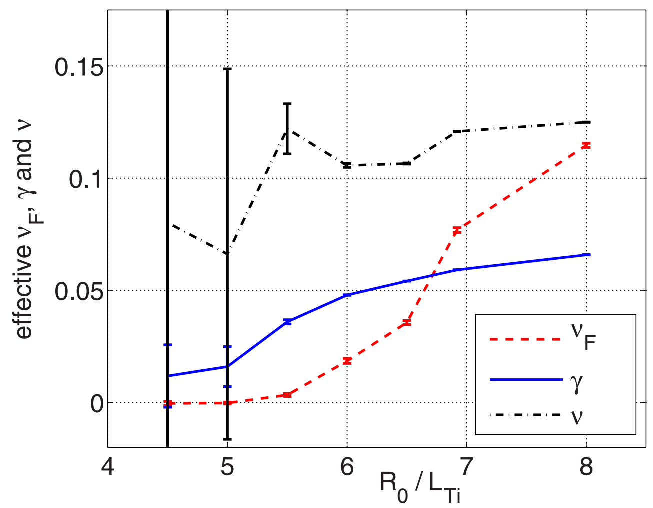

Figure 5. Effective ZFs dissipation (ν_F, the solid line), growth rate (γ, the dashed line) and small-scale dissipation (ν, the dotted line) as functions of R_0/L_{T_i}, with hyperdiffusion GyroLES ($c_\perp = 0.5$). An error estimate is given by the standard deviation of the free energy time traces.

2. The small-scale dissipation ν (dotted lines) is found to be approximately constant, except for small values of the temperature gradient. γ and surprisingly ν_F display a nontrivial dependence with R_0/L_{T_i}, very similar to the heat flux structure found in other studies [49].

In order to verify equations (14) and (15), the averaged free energy ratios $\langle\mathcal{E}_1\rangle/\langle\overline{\mathcal{E}}\rangle$ and $\langle\mathcal{E}_2\rangle/\langle\overline{\mathcal{E}}\rangle$ are represented as functions of the ratios ν_F/ν and ν_F/γ respectively in figure 6. Six series of GyroLESs are considered, varying the diffusion or hyperdiffusion amplitudes, the temperature gradient R_0/L_{T_i}, as well as the magnetic shear, for a total of 40 nonlinear GyroLESs. The advantage of using LES for these simulations, (apart from the gain in speed) is that it provides an easy handle on the small-scale dissipation via $c_\perp$ and allows us to modify ν independently in order to explore the parameter space easily.

The curves seem to agree with the theoretically predicted ratios in equations (14) and (15). Results are however found to depart from the theory when the turbulence level is decreased, especially in the low-shear case and for very high perpendicular dissipation amplitudes. These disagreements correspond to the limit of the GyroLES technique when the chosen grid cannot capture completely the linear physics (low shear), or when the GyroLES sub-grid model amplitude $c_\perp$ is not strong enough to compensate the lack of resolution. The deviation of the ratio $\mathcal{E}_1/\overline{\mathcal{E}}$ from a straight line, is rather small, while it is more pronounced for $\mathcal{E}_2/\overline{\mathcal{E}}$. Again this could be due to the reduction of the size of the dissipative range, by the GyroLES technique, which affects mainly the small scales associated to $\mathcal{E}_2$.

In order to compare the reduced predator–prey model (8), (9), (10), with the results of nonlinear gyrokinetic simulations, the appropriate parameter space is given by the three parameters γ, ν_F and ν. Considering the different temperature gradient scans obtained with DNS, or two different GyroLES models ($c_\perp = 0.5$ and $c_\perp = 0.375$), the ratio ν_F/γ is observed to be approximately constant: table 1 summarizes the numerical values obtained.

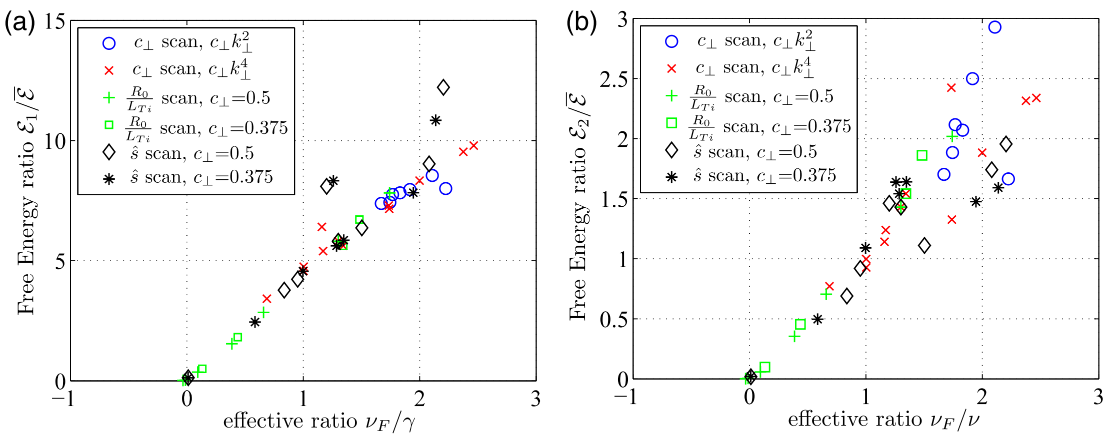

Figure 6. Free energy ratios ($\mathcal{E}_1/\overline{\mathcal{E}}$ (a), $\mathcal{E}_2/\overline{\mathcal{E}}$ (b)) as functions of the ratio between the effective ZF dissipation, the effective growth rate and the effective small-scale dissipation (see equations (14) and (15)). Blue circles and red crosses stand respectively for diffusion and hyperdiffusion GyroLES model scanned along $c_\perp$, green plus and squares represent two R_0/L_{T_i} scans, with respectively $c_\perp = 0.5$ and $c_\perp = 0.375$ chosen for hyperdiffusion GyroLES. Black diamonds and stars correspond to a magnetic shear scan $\hat{s}$ with respectively $c_\perp = 0.5$ and $c_\perp = 0.375$.

Table 1. Ratios ν/γ and ν_F/γ, for different values of the temperature gradient R_0/L_{T_i}, and with different numerical methods. LES#1 and LES#2 correspond to $c_\perp = 0.375$ and $c_\perp = 0.5$, respectively (hyperdiffusion model $n = 2$). An error estimate is given by the standard deviation of the free energy time traces.

R_0/L_{T_i}	6.0	6.92	8.0
ν/γ, DNS	2.05 ± 0.01	2.01 ± 0.01	2.35 ± 0.01
ν/γ, LES#1	1.99 ± 0.01	1.64 ± 0.01	1.70 ± 0.01
ν/γ, LES#2	2.23 ± 0.03	2.03 ± 0.01	1.90 ± 0.01
ν_F/γ, DNS	0.25 ± 0.01	0.39 ± 0.01	0.49 ± 0.01
ν_F/γ, LES#1	0.44 ± 0.03	1.34 ± 0.01	1.48 ± 0.01
ν_F/γ, LES#2	0.39 ± 0.03	1.30 ± 0.02	1.74 ± 0.02

It is then possible to normalize the predator–prey system (8), (9), (10) by γ, and to obtain

$$\partial_{t'}\overline{\mathcal{E}} = \overline{\lambda}'\overline{h}h_1h_2 - \frac{\nu_F}{\gamma}\overline{\mathcal{E}}, \tag{16}$$

$$\partial_{t'}\mathcal{E}_1 = \lambda_1'\overline{h}h_1h_2 + \mathcal{E}_1, \tag{17}$$

$$\partial_{t'}\mathcal{E}_2 = \lambda_2'\overline{h}h_1h_2 + \frac{\nu}{\gamma}\mathcal{E}_2, \tag{18}$$

where the time has been normalized $t' = \gamma t$, as well as the geometric prefactors $\overline{\lambda}' = \overline{\lambda}/\gamma$, $\lambda_1' = \lambda_1/\gamma$ and $\lambda_2' = \lambda_2/\gamma$. As suggested from the results presented in table 1, the ratio ν/γ can be considered approximately constant, and the only free parameter remaining is ν_F/γ. A simple comparison is then possible between the normalized system (16), (17), (18), and the nonlinear gyrokinetic simulations.

In figure 7, the local maxima of the ZFs free energy $\overline{\mathcal{E}}$ are represented as a function of the normalized ZF damping coefficient ν_F/γ. In light gray, results obtained by solving the reduced predator–prey system are given, where each point corresponds to a local maximum in the time trace of the ZF free energy $\overline{\mathcal{E}}$. In the simple predator–prey model, two distinct regimes are obtained: periodic oscillations, with well-defined amplitudes for the highest values of the parameter ν_F/γ, and a chaotic regime occurs when decreasing the parameter ν_F/γ.

Results obtained with nonlinear gyrokinetic simulations are shown in figure 7 together with the bifurcation diagram. For each simulation, mean, maximum and minimum values give the error bar representation used in the figure.

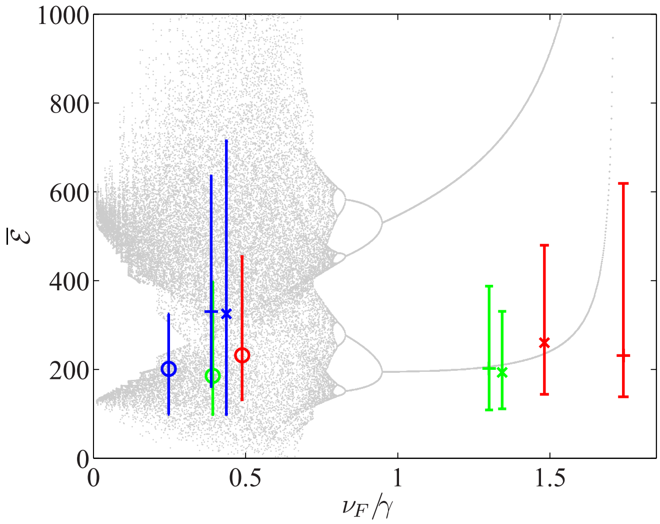

Figure 7. Bifurcation diagram showing the local maxima of $\overline{\mathcal{E}}$ as a function of ν_F/γ, obtained from simple predator–prey model (light gray), as described in [9], compared with DNS (o) and two different GyroLES models ($\times$ for LES#1 and + for LES#2). Three different values $R_0/L_{T_i} = 6.0;\ 6.92;\ 8.0$ are considered (respectively, blue, green and red).

5. Discussion

We have performed a detailed characterization of the dynamics and the associated spectral transfer, using the evolution of free energy in gyrokinetic turbulence with a partition of the k-space corresponding to the scales of free energy injection, free energy dissipation and large-scale flow structures.

This study provides, yet another indication that the predator–prey-like dynamical interactions between large-scale flows and the micro-turbulence responsible from the anomalous transport is an inherent part of plasma micro-turbulence. The approach that is used in this work, namely local, adiabatic electron, GyroLESs of ITG turbulence, is not the most complete description of plasma turbulence. However it is sufficiently representative of core plasma turbulence and allows us additional handle on the diffusivities due to effective diffusive or hyperdiffusive terms introduced in the LES formulation which permits the detailed scans shown in this paper.

Our results show in particular that the free energy exchange between the three partitions, mentioned above, exhibits many of the well-known characteristic features of the predator–prey dynamics. The ZF free energy $\overline{\mathcal{E}}$ has been shown to be phase delayed in time with respect to the turbulent free energy $\widetilde{\mathcal{E}}$. Statistics of the turbulent free energy as a function of the binormal wavenumber k_y show rather different characteristics between small Gaussian scales and large scales with an intermittent behavior.

These observations provide physical insight and a justification for the use of a simple reduced three population model of plasma micro-turbulence, based on gyrokinetic DNSs. This reduced model has been tested with gyrokinetic numerical experiment, and we have shown that the predicted relation between the average amplitudes of the different free energy components as given in equations (14) and (15) holds reasonably well in gyrokinetic simulations.

The role of predator–prey-like dynamics on the L–H transition remains an open question. As of today, full physics gyrokinetic simulations cannot tackle the L–H transition or the intermediate phase with limit cycle oscillations. This means such problems have to be considered using simple transport models that include mesoscale physics such as ZFs, turbulence spreading or even some simple cascade model. Such models have to be justified by comparing their limiting predictions to gyrokinetic simulations or experimental observations. Development of such advanced mesoscale/transport models will be one of the important theoretical activities in the upcoming years.

Acknowledgments

The authors would like to thank F Jenko and T Görler for the use of the GENE code, A Banón Navarro and D Carati for fruitful discussions and acknowledge that the nonlinear gyrokinetic simulations presented in this work have been achieved with the assistance of high performance computing resources on the HPC-FF systems at Jülich, Germany, and the JADE supercomputer, CINES, Montpelier, France. This work is supported by the French Agence nationale de la recherche, contract ANR JCJC 0403 01 and by the contract of association EURATOM-Belgian state.

References

[1] Goel N S, Maitra S C and Montroll E W 1971 *Rev. Mod. Phys.* **43** 231
[2] Malkov M A, Diamond P H and Rosenbluth M N 2001 *Phys. Plasmas* **8** 5073
[3] Kim E J and Diamond P H 2003 *Phys. Plasmas* **10** 1698
[4] Estrada T, Happel T, Hidalgo C, Ascasibar E and Blanco E 2010 *Europhys. Lett.* **92** 35001
[5] Conway G D, Angioni C, Ryter F, Sauter P and Vicente J (ASDEX Upgrade Team) 2011 *Phys. Rev. Lett.* **106** 065001
[6] Zhao K J *et al* 2010 *Plasma Phys. Control. Fusion* **52** 124008
[7] Smolyakov A I, Diamond P H and Shevchenko V I 2000 *Phys. Plasmas* **7** 1349
[8] Gürcan Ö D, Garbet X, Hennequin P, Diamond P H, Casati A and Falchetto G L 2009 *Phys. Rev. Lett.* **102** 255002
[9] Berionni V and Gürcan Ö D 2011 *Phys. Plasmas* **18** 112301
[10] Lin Z, Hahm T S, Lee W W, Tang W M and White R B 1998 *Science* **281** 1835
[11] Wang W X, Lin Z, Tang W M, Lee W W, Ethier S, Lewandowski J L V, Rewoldt G, Hahm T S and Manickam J 2006 *Phys. Plasmas* **13** 092505
[12] Waltz R E, Candy J and Fahey M 2007 *Phys. Plasmas* **14** 056116
[13] Dif-Pradalier G, Grandgirard V, Sarazin Y, Garbet X and Ghendrih P 2009 *Phys. Rev. Lett.* **103** 065002
[14] Nakata M, Watanabe T-H and Sugama H 2012 *Phys. Plasmas* **19** 022303
[15] Morel P, Bañòn Navarro A, Albrecht-Marc M, Carati D, Merz F, Görler T and Jenko F 2011 *Phys. Plasmas* **18** 072301
[16] Terry P W *et al* 2012 *Phys. Plasmas* **19** 055906
[17] Hatch D, Terry P W, Jenko F, Merz F and Nevins W M 2011 *Phys. Rev. Lett.* **106** 115003
[18] Morel P, Bañòn Navarro A, Albrecht-Marc M, Carati D, Merz F, Görler T and Jenko F 2012 *Phys. Plasmas* **19** 012311
[19] Catto P J 1978 *Plasma Phys.* **20** 719
[20] Littlejohn R G 1982 *J. Math. Phys.* **23** 742
[21] Frieman E A and Chen L 1982 *Phys. Fluids* **25** 502
[22] Dubin D H E, Krommes J A, Oberman C and Lee W W 1983 *Phys. Fluids* **26** 3524
[23] Lee W W 1983 *Phys. Fluids* **26** 556
[24] Hahm T S 1988 *Phys. Fluids* **31** 2670
[25] Hahm T S 1996 *Phys. Plasmas* **3** 4658
[26] Sugama H 2000 *Phys. Plasmas* **7** 466
[27] Brizard A J 2000 *Phys. Plasmas* **7** 4816
[28] Schekochihin A A, Cowley S C, Dorland W, Hammett G W, Howes G G, Plunk G G, Quataert E and Tatsuno T 2008 *Plasma Phys. Control. Fusion* **50** 124024
[29] Scott B and Smirnov J 2010 *Phys. Plasmas* **17** 112302
[30] Parra F I and Catto P J 2010 *Phys. Plasmas* **17** 056106
[31] Lee W W, Dong J Q, Guzdar P N and Liu C S 1987 *Phys. Fluids* **30** 1331
[32] Brizard A J and Hahm T S 2007 *Rev. Mod. Phys.* **79** 421
[33] Garbet X, Idomura Y, Villard L and Watanabe T H 2010 *Nucl. Fusion* **50** 043002
[34] Krommes J A 2012 *Annu. Rev. Fluid Mech.* **44** 175
[35] Dannert T and Jenko F 2005 *Phys. Plasmas* **12** 072309
[36] Lapillonne X, Brunner S, Dannert T, Jolliet S, Marinoni A, Villard L, Görler T, Jenko F and Merz F 2009 *Phys. Plasmas* **16** 032308
[37] Pueschel M J, Dannert T and Jenko F 2010 *Comput. Phys. Commun.* **181** 1428
[38] Jenko F, Dorland W, Kotschenreuther M and Rogers B N 2000 *Phys. Plasmas* **7** 1904
[39] Görler T, Lapillonne X, Brunner S, Dannert T, Jenko F, Merz F and Told D 2011 *J. Comput. Phys.* **230** 7053
[40] Watanabe T-H and Sugama H 2006 *Nucl. Fusion* **46** 24
[41] Candy J and Waltz R E 2006 *Phys. Plasmas* **13** 032310
[42] Tatsuno T, Dorland W, Schekochihin A A, Plunk G G, Barnes M, Cowley S C and Howes G G 2009 *Phys. Rev. Lett.* **103** 015003
[43] Bañòn Navarro A, Morel P, Albrecht-Marc M, Carati D, Merz F, Görler T and Jenko F 2011 *Phys. Plasmas* **18** 092303
[44] Bañón Navarro A, Morel P, Albrecht-Marc M, Carati D, Merz F, Görler T and Jenko F 2011 *Phys. Rev. Lett.* **106** 055001
[45] Diamond P H, Itoh S-I, Itoh K and Hahm T S 2005 *Plasma Phys. Control. Fusion* **47** R35
[46] Rhines P B and Young W R 1982 *J. Fluid Mech.* **122** 347
[47] Diamond P H, Gürcan Ö D, Hahm T S, Miki K, Kosuga Y and Garbet X 2008 *Plasma Phys. Control. Fusion* **50** 124018
[48] Krommes J A and Kim C B 2000 *Phys. Rev.* E **62** 8508
[49] Dimits A M, Bateman G, Beer M A, Cohen B I, Dorland W, Hammett G W, Kim C, Kinsey J E, Kotschenreuter M and Kritz A H 2000 *Phys. Plasmas* **7** 969
[50] DeCarlo L T 1997 *Psychol. Methods* **2** 292